Metrol. Meas. Syst., Vol. 31 (2024) No. 2, pp. 323–338
DOI: 10.24425/mms.2024.149695

PAN POLSKA AKADEMIA NAUK

METROLOGY AND MEASUREMENT SYSTEMS
Index 330930, ISSN 0860-8229
www.metrology.wat.edu.pl

M&MS

A NOVEL ULTRA-LOW-FREQUENCY MICRO-VIBRATION CALIBRATION METHOD BASED ON VIRTUAL PENDULUM MOTION TRAJECTORIES OF THE STEWART PLATFORM

Tong Ye[1)], Zhihua Liu[2)], Chenguang Cai[2)], Fubing Bao[1)], Fei Xu[1)], Xiangkun Lian[1)]

1) College of Metrology and Measurement Engineering, China Jiliang University, 310018 Hangzhou, China
2) Institute of Mechanics and Acoustic Metrology, National Institute of Metrology, 100029 Beijing, China
(✉ *liuzhihua@nim.ac.cn*)

Abstract

Micro-acceleration generation during ultra-low-frequency micro-vibration calibration is a sensitive issue. There are issues of traditional pendulum tables being unable to change the pendulum radius and direction to produce micro-accelerations of different magnitudes, and the line shakers having a low signal-to-noise ratio when the vibration amplitude is the same as that of the pendulum tables. Therefore, a novel ultra-low-frequency micro-vibration calibration method is proposed to solve the above issues based on virtual pendulum motion trajectories of the Stewart platform. The micro-accelerations of 10^{-5} to 10^{-3} m/s^2 can be generated by the trajectories with the radius of up to 12 m, the displacement amplitudes of up to 11.636 mm and the frequencies between 0.01 and 0.1 Hz. In the virtual pendulum motion, the maximum acceleration can be 2481 times greater than the acceleration of linear motion at the same frequency and displacement amplitude. In a comparison experiment with the current rotating platform, the maximum relative deviation of sensitivity amplitude calibration for pendulum motion around the x- and y-axis based on the Stewart platform are 0.411% and 0.295% respectively. The above results demonstrate the validity and reliability of this kind of method.

Keywords: micro-vibration calibration, Stewart platform, ultra-low frequency, virtual pendulum motion trajectories.

1. Introduction

Sensors sensitive to *ultra-low frequency micro-vibration* (ULFMV) are widely applied in the fields of earthquake observation, environmental monitoring, geological exploration as well as space navigation of large-scale space structures and monitoring and fault prediction of spacecraft engines. For example, the "Hubble" space telescope could not work properly after it was put into orbit due to micro-vibrations which have a frequency response in the range of DC–10 Hz [1–4]. Micro-vibration calibration of the sensor is a prerequisite for ensuring accurate, reliable, and effective measurement data. Therefore, the demand for sensitivity calibration has become extremely urgent [5, 6].

Article history: received November 20, 2023; revised January 19, 2024; accepted February 2, 2024; available online March 7, 2023.

Micro-vibration calibration of sensors requires exciters, such as shakers, to provide them with micro vibration excitation. In the ULFMV reference devices, the ultra-low frequency standard shaker used for inspection and calibration is the core of the entire calibration system. In terms of the rotating platform, the National Institute of Metrology of Japan can generate micro-accelerations of 10^{-3}–10^{-2} m/s^2 based on it, with a minimum frequency of 0.1 Hz [7]. However, it is easy to cause wire winding and it also entails the application of slip rings during the use of the rotating platform, which can easily interfere with the signal and require precision processing and debugging resulting in high process requirements and high costs. In terms of the linear shaker, the National Measurement Institute of Australia has established a long-stroke linear shaker with a maximum displacement of no more than 160 mm, a vibration frequency of 0.5 to 20 Hz, and an effective load of 3 kg [8]. The low-frequency standard shaker based on linear motors established by the National Institute of Metrology of China has a frequency range of 0.01 to 100 Hz, an acceleration range of 1.580×10^{-3} to 10 m/s^2, and a maximum amplitude of 400 mm [9–11]. However, since the acceleration of the linear shaker is proportional to the frequency squared and vibration displacement amplitude, there is a problem of low signal-to-noise ratio in calibrating acceleration in the case of ultra-low frequency when the displacement amplitude is fixed. As a result, all conventional 1D micro-vibration calibration methods have serious drawbacks when applied.

At present, *Changcheng Institute of Metrology & Measurement of China* (CIMM) has an ultra-low-frequency acceleration calibration device [12], the most important component of which is a physical pendulum table with a circular air-bearing guide. The pendulum radius is fixed at 10 m, the maximum swing displacement is 10 mm, and the operating frequency range is 0.001–0.1 Hz. When the frequency is 0.001 Hz, the maximum acceleration can reach 1×10^{-2} m/s^2, which is equivalent to a linear vibration table with an amplitude of 254 m. The ycГ-3 micro-acceleration calibration device of the D.I. Mendeleev All-Russian Institute for Metrology (VNIIM) can achieve vibration calibration with a frequency range of 0.001–30 Hz and an acceleration amplitude range of 5×10^{-7}–2 m/s^2, using a physical pendulum table with a curvature radius of 10 m [13]. However, the traditional 10 m radius pendulum table cannot change the designed pendulum radius. If changes are needed, the mechanical components of the system need to be re-designed and manufactured, which lacks universality.

In recent years, shakers have become popular in research by generating plane or spatial motion trajectories for vibration calibration [14]. On the one hand, generating various motion trajectories can achieve multi-axis simultaneous measurement, avoid errors caused by multiple sensor installations during single-axis calibration, and improve calibration accuracy [15]. On the other hand, it expands the scope of calibration and is no longer limited to linear vibration calibration. M. Yang *et al.* [16] proposed a planar elliptical orbit excitation accelerometer sensor based on a tri-axial sensor calibration system. Z. Liu *et al.* [17] developed a test method that determines the lateral sensitivity of sensors based on multi-axis spatial elliptical trajectories and spatial spherical motion trajectories based on a tri-axial vibration exciter [18], where spatial circular trajectories and spatial linear trajectories are two special cases of spatial elliptical trajectories. Nevertheless, tri-axial vibration excitation systems can only achieve linear motion in the plane for line vibration calibration, but not for angular vibration calibration. In 2023, Q. Yang *et al.* [19, 20] worked out a dynamic testing method for MEMS inclinometers based on spatial conical motion trajectories of the Stewart platform, which accelerates the angle drift of MEMS inclinometers and can realize classic conical motion, attitude conical motion, and synthesis of the conical motion trajectories. However, based on the above motion trajectories, the ULFMV cannot be achieved. In conjunction with the previously mentioned pendulum motion, we hypothesized that ULFMV calibration can be achieved based on the pendulum motion trajectories of the Stewart platform.

Metrol. Meas. Syst., Vol. 31 (2024), No. 2, pp. 323–338
DOI: 10.24425/mms.2024.149695

Therefore, this paper presents an ULFMV calibration method based on the *virtual pendulum motion trajectory* (VPMT) of the Stewart platform. Micro-accelerations of different magnitudes are generated and regulated by VPMTs of different radii and directions. The Stewart platform can achieve VPMTs around the x- and y-axis, with a maximum virtual radius of up to 12 m. The micro-vibration calibration system breaks through the structural and performance limitations of the classical pendulum table and linear vibration shaker. It adopts a unique structure that allows for changing the virtual pendulum radius, which increases the displacement amplitude when limiting the small pendulum angle to improve the accuracy of micro-vibration calibration.

This paper investigates a novel ULFMV method based on VPMTs of the Stewart platform. The organizational structure of this paper is as follows: Section 2 introduces the ULFMV based on the VPMTs. Section 3 discusses the VPMTs of the Stewart platform. Section 4 presents the sensor calibration results under ULFMV. Section 5 ends with the conclusions.

2. Ultra-low frequency micro-vibration based on virtual pendulum motion trajectories

The principle of the pendulum motion [21,22] is shown in Fig. 1, and the particle H makes arks along the pendulum r in the vertical plane. The swinging displacement is A, and the displacement amplitude is A_0. The swinging angle is φ, and the swinging angle amplitude is φ_0. The vibration frequency is f, and the angular velocity is ω.

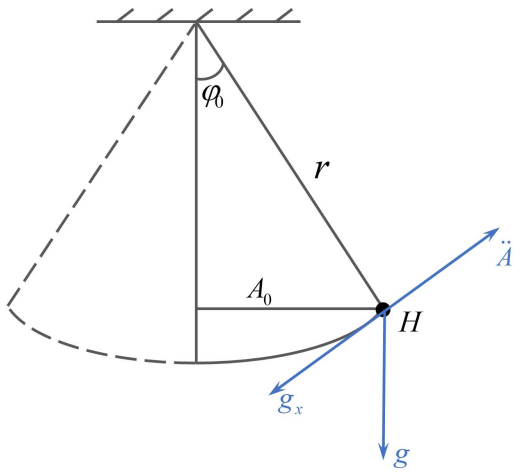

Fig. 1. The principle of the pendulum motion.

According to the principle of pendulum motion, micro-acceleration generated by the VPMT is composed of two parts, namely the component of gravitational acceleration along the direction of motion and the acceleration of pendulum tangential vibration provided by the Stewart platform. Due to the acceleration brought by the latter, the vibration can be triggered even when the excitation frequency is far lower than the natural frequency f_0 which is defined as $f_0 = (2\pi\sqrt{g/r})^{-1}$. As shown in Fig. 2, when the radius of the virtual pendulum is 1, 5, 10, and 12 m, the natural frequency of the virtual pendulum is the lowest at 0.144 Hz, so a certain reverse excitation must be given by the Stewart platform. The actual excitation acceleration peak of the vibration sensor is given by

$$a = g_x - \ddot{A}, \tag{1}$$

where $g_x$is the component of gravitational acceleration along the direction of motion and $\ddot{A}$ is the vibration excitation acceleration provided by the Stewart platform, in which g_x and $\ddot{A}$ are expressed as

$$g_x = g \sin \varphi, \tag{2}$$

$$\ddot{A} = \frac{\mathrm{d}^2(A_0 \sin \omega t)}{\mathrm{d}t^2}, \tag{3}$$

where $g = 9.8015$ m/s^2 is the local gravity acceleration.

As the swinging angle is very small (less than 200″), the relative error between the swing angle and its sinusoidal value is less than 1.567×10^{-7}, and the swing angle can be considered equal to its sinusoidal value [22], that is

$$\varphi_0 = \sin \varphi_0 = \frac{A_0}{r}. \tag{4}$$

Substituting (4) into (1) yields

$$a = \left(\frac{gA_0}{r} - A_0 \omega^2 \right) \sin \omega t, \tag{5}$$

where the amplitude of the sinus motion in (5) is given by

$$a_0 = \left(\frac{g}{r} - \omega^2 \right) A_0. \tag{6}$$

According to (6), when $f = 0.01$ Hz, $\varphi_0 = 200''$, the item $\omega^2 A_0$ tends to 0. At this time, the VPMTs acceleration is almost only produced by gravity and is independent of frequency. Compared with $f = 0.01$ Hz, when $f = 0.1$ Hz, $r = 12$ m, the VPMTs acceleration decreased by 48.083%. At $r = 10, 5$ and 1 m, the acceleration fell by 40.036%, 19.978% and 3.989%, respectively. In particular, when $f = 0.01$ Hz and $r = 12$ m, the displacement amplitude of 209.440 μm can reproduce an acceleration of 8.839×10^{-5} m/s^2. When the frequency increases to the natural frequency, $\omega^2 A_0$ and gA_0/r are equal, and the virtual pendulum acceleration output tends to 0. It can be seen that in the working frequency range of 0.01–0.1 Hz, the generation of standard acceleration is mainly dominated by the gravity of the virtual pendulum, and the Stewart platform, as a vibration exciter, also provides a partial power source.

Micro-accelerations of different magnitudes can be obtained by varying the frequency and radius. The amplitude-frequency characteristics are shown in Fig. 2.

The Stewart platform provides vibration excitation acceleration that is equivalent to the linear motion acceleration whose displacement is the same as that of the pendulum motion, *i.e.*,

$$a' = a_0 + \ddot{A} = \frac{gA_0}{r}. \tag{7}$$

According to (4) and (7), A_0 is immutable when the virtual pendulum radius r is constant and the angle φ is fixed. Therefore, the gravitational acceleration along the motion direction is constant and always greater than 0. At the same motion displacement, compared with linear motion, the virtual pendulum motion can produce greater micro-acceleration.

Metrol. Meas. Syst., Vol. 31 (2024), No. 2, pp. 323–338
DOI: 10.24425/mms.2024.149695

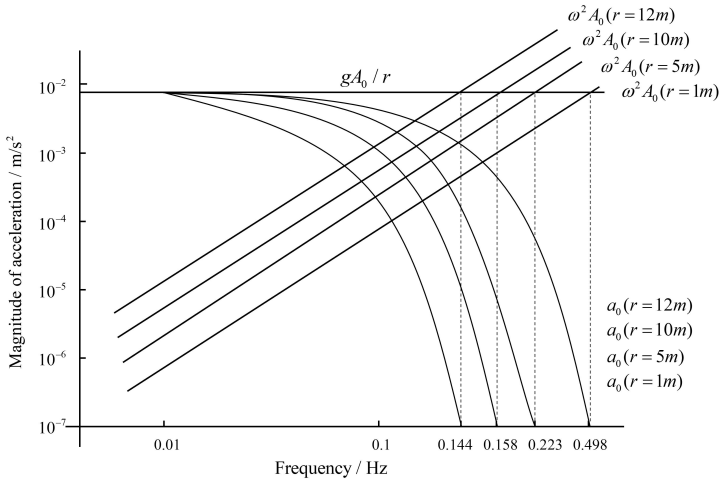

Fig. 2. Magnitude-frequency characteristic of the Stewart platform.

3. Virtual pendulum motion trajectories of the Stewart platform

In order to verify that the Stewart platform can realize the VPMTs, an ULFMV calibration system was built as shown in Fig. 3. The system consists of a VPMTs generation device (the Stewart Platform), the VPMTs measurement system (camera (Aicon 3D MoveInspect XR8), target and receiver [23]), sensors calibration system (*data acquisition* (DAQ) card (INV 3062-C), a VSE355G3 calibrated sensor, *quartz flexible accelerometer* (QFA)) and a host computer. The sensors and targets are fastened to the motion platform of the Stewart platform using screws and adhesives. Screw mounting is a rigid connection that reduces the motion of the transducer relative to the shaker and reduces calibration uncertainty [24]. The voltage signals of sensor [25] are acquired through a 24-Bit DAQ card by setting 20 times filtering and 50 times sampling frequency. We obtained a signal with good waveforms with less than 5% distortion. The camera is used to capture and record the pose changes of the target following the motion platform during the VPMTs at different positions. According to the Hexagon MoveInspect XR8 7.16 manual, the accuracy of camera is 40 μm [26–28], and the VPMTs has a maximum displacement of 11.636 mm and a minimum of 209.440 μm, which satisfies the measurement range of the measurement system.

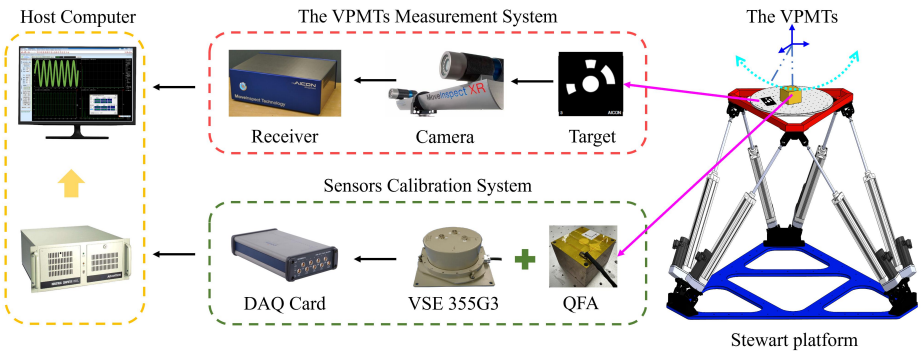

Fig. 3. The ULFMV calibration system based on the Stewart platform.

The Stewart platform, as a motion generator, is the core part of the whole calibration system. It is a multi-degree-of-freedom motion equipment that can accurately realize complex motions and has a bearing capacity of 100 kg. It mainly consists of a base platform, a motion platform, and six telescopic branches. The two ends of the telescopic branch are respectively connected to the base platform and the motion platform via Hooke joints. By changing the length of the telescopic branch, the motion platform can achieve different poses The Stewart platform can provide vibration excitation acceleration in the range of 0.01 to 0.1 Hz, a maximum peak-to-peak excitation displacement of 600 mm, and the maximum motion angle of 25°. As a result, it is capable of realizing the VPMTs with variable radius.

The accuracy of the motion trajectory of the Stewart platform is tested by using the RLE fiber optic laser encoder. The Stewart platform performs 20 tests along the x- and y-axis from 0 to 50 mm to verify whether it can accurately move to the specified position. The test results showed that the average values of the 20 motion tests along the x- and y-axis directions were 50.036 mm and 50.025 mm, with standard deviations of 0.824 μm and 0.712 μm, respectively. This indicates that the motion trajectory of the Stewart platform is accurate.

The control system of the Stewart platform is shown in Fig. 4. The host computer starts the VPMTs planning after inputting the parameters r, f, and A_0 required for pendulum motion and then runs the motion program. The pose information obtained from the motion program is used to calculate through inverse kinematics to get the leg length command value L_i ($i = 1 \ldots 6$) and then to inform the servo drivers. Servo drives control the movement of servo motors. Finally, the Stewart platform outputs VPMTs.

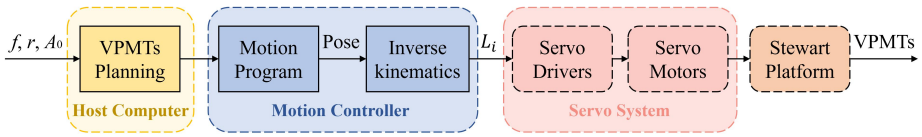

Fig. 4. Control system of the Stewart platform.

As any periodic function can be decomposed into sine functions [29], to simulate the VPMTs on the Stewart platform, the coordinate system of the moving platform needs to be established at a height r above the geometric center of the moving platform tabletop, where r is the radius of the virtual pendulum. This is markedly different from the way other spatial motions establish coordinate systems. Other spatial motions usually establish the coordinate system only at the geometric center of the motion platform's tabletop. Otherwise, the position and orientation will change during the pendulum motion and become indescribable. Establishing the coordinate system using the mentioned method, only the angle variation around a certain axis during the VPMT is necessary. Thus, the spatial pendulum motion can be represented as

$$\begin{cases} A' = A_x \sin\left(2\pi f_x t + \varphi_x\right) \\ B' = B_y \sin\left(2\pi f_y t + \varphi_y\right) \end{cases}, \tag{8}$$

where A' and B', f_x and f_y represent the sinusoidal and variations of the angles around the x- and y-axis, respectively, and φ_x and φ_y represent the phases.

As shown in Fig. 5a, the VPMT is in the xoz plane, that is, around the y-axis, and the swing angle amplitude A_x. As shown in Fig. 5b, O is the origin of the base platform coordinate system O–xyz located at the geometric center of the base platform. P' is the origin of the motion platform coordinate system, located at point P, the geometric center of the motion platform, at a height of r along the z-axis. The z-axis is perpendicular to the surface of the motion platform. The Hooke joint

Metrol. Meas. Syst., Vol. 31 (2024), No. 2, pp. 323–338
DOI: 10.24425/mms.2024.149695

coordinates on the base platform can be described by the translation and rotation transformation of the $P' - xyz$ motion platform coordinate system relative to the O-xyz base platform coordinate system, which can be expressed in the form of (9). The origin coordinates P' of the motion platform coordinate system can be expressed as $\boldsymbol{T} = (x, y, z)$, while $\boldsymbol{p}_i = (X_{pi}, Y_{pi}, Z_{pi})$ $(i = 1 \ldots 6)$ is the coordinate of the i-th Hooke joint on the base platform in the O-xyz coordinate system, which is the absolute coordinate and $\boldsymbol{b}_i = (X_{bi}, Y_{bi}, Z_{bi})$ $(i = 1 \ldots 6)$ is the coordinate of the i-th Hooke joint on the motion platform in the P'–xyz coordinate system. OP' is the vector from the origin O of the base platform coordinate system to the origin $P'$of the motion platform coordinate system. ${}^{v}\boldsymbol{p}_i = (x_{pi}, y_{pi}, z_{pi})$ $(i = 1 \ldots 6)$ is the coordinate of the i-th Hooke joint on the motion platform in the O-xyz base platform coordinate system, which is the relative coordinate [27, 28, 30]. Based on the above transformations, the coordinate of the Hooke joint $\boldsymbol{p}_i$ relative to the O-xyz base platform coordinate system can be written as

$$\boldsymbol{p}_i = \boldsymbol{R} \cdot {}^{v}\boldsymbol{p}_i + \boldsymbol{t} \tag{9}$$

or

$$\begin{bmatrix} X_{pi} \\ Y_{pi} \\ Z_{pi} \\ 1 \end{bmatrix} = \begin{bmatrix} \boldsymbol{R} & \boldsymbol{t} \\ 0 & 1 \end{bmatrix} \begin{bmatrix} x_{pi} \\ y_{pi} \\ z_{pi} \\ 1 \end{bmatrix}. \tag{10}$$

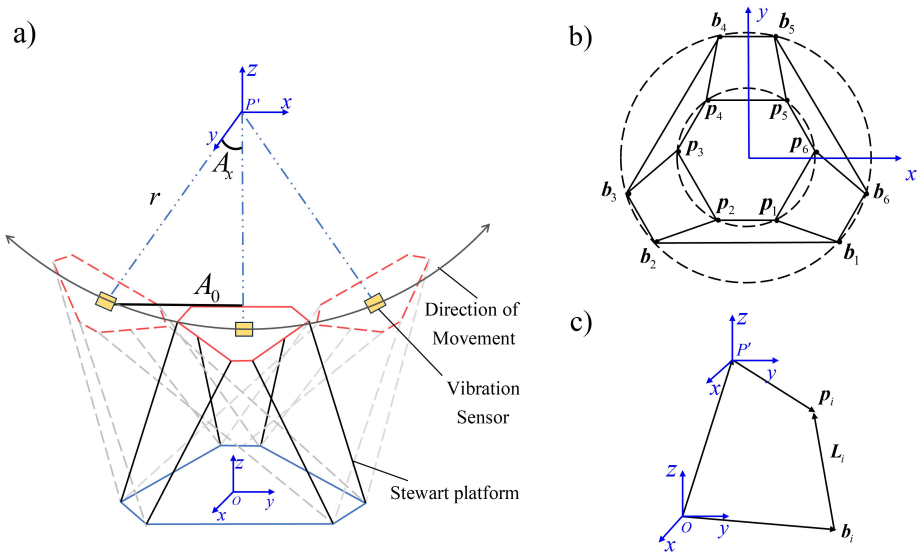

Fig. 5. The principle of VPMTs generated by the Stewart platform: a) the VPMTs model based on a Stewart platform; b) coordinate transformation; c) vector closed-loop diagram.

In the (10), $\boldsymbol{t}$ represents the translation transformation vector of the motion platform coordinate system in the base platform coordinate system. $\boldsymbol{R}$ represents the combined transformation matrix of the motion platform pose described by Euler angles. The motion platform coordinate system begins to rotate by angle αaround the z-axis of the motion platform coordinate system, then rotates by angle β around the y-axis of the motion platform coordinate system, and finally rotates by angle γ around the x-axis of the motion platform coordinate system. The elements of the three column vectors $(\boldsymbol{I}_x, \boldsymbol{I}_y, \boldsymbol{I}_z)^T$, $(\boldsymbol{J}_x, \boldsymbol{J}_y, \boldsymbol{J}_z)^T$ and $(\boldsymbol{K}_x, \boldsymbol{K}_y, \boldsymbol{K}_z)^T$ of the rotation matrix $\boldsymbol{R}$ are the

projections of the unit vectors on the coordinate axis of the moving coordinate system onto the base coordinate system. In the right-handed coordinate system, the combined rotation matrix $\boldsymbol{R}$ can be represented as

$$\boldsymbol{R} = \boldsymbol{R}(z,\alpha)\boldsymbol{R}(y,\beta)\boldsymbol{R}(x,\gamma) = \begin{pmatrix} c\alpha c\beta & c\alpha s\beta s\gamma - s\alpha c\gamma & c\alpha s\beta c\gamma + s\alpha s\gamma \\ s\alpha c\beta & s\alpha s\beta s\gamma + c\alpha c\gamma & s\alpha s\beta c\gamma - c\alpha s\gamma \\ -s\beta & c\beta s\gamma & c\beta c\gamma \end{pmatrix}. \tag{11}$$

in which c means cos, s means sin.

As shown in Fig. 5c, according to the closed-loop vector formula, the branch elongation L_i can be obtained [31], that is:

$$\boldsymbol{L}_i = \boldsymbol{R} \cdot {}^{v}\boldsymbol{p}_i + \boldsymbol{t} - \boldsymbol{b}_i. \tag{12}$$

Kinematic inverse solution can obtain the unique solution of the telescopic branch through pose, which serves as the control signal input of the Stewart platform to realize the VPMTs.

4. Sensor calibration results under ultra-low frequency micro-vibration

4.1. Comparison between the virtual pendulum and linear motion trajectories

Experiments were performed based on the calibration system from Fig. 6. Two sensors were used to verify different two issues. One is the VSE-355G3 servo-type velocity sensor with a known sensitivity, manufactured by Tokyo Measuring Instruments, which was used to compare the micro-acceleration generated by pendulum and linear motion. The other is a quartz flexural accelerometer with an unknown sensitivity, which was used for calibration due to its high measurement accuracy and stable performance in ultra-low frequency situations.

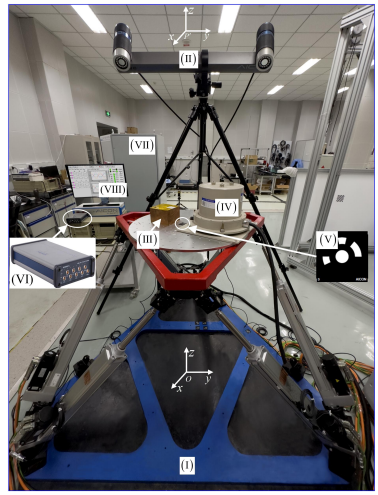

Fig. 6. Sensor micro-vibration calibration system: (I) Stewart platform; (II) camera; (III) QFA; (IV) VSE-355G3; (V) target; (VI) DAQ card; (VII) control cabinet; (VIII) host computer.

To verify that the pendulum motion of the Stewart platform can generate larger acceleration compared to linear motion and improve the signal-to-noise ratio, the VSE-355G3 with a known sensitivity of 5000 mV/(m/s^2) and a weight of 27 kg was selected. Under the condition of the

same vibration displacement, the Stewart platform provides vibration excitations with vibration frequencies of 0.01 to 0.1 Hz for pendulum motion and linear motion. The swing angle of the pendulum is 200″, and the radius is 1, 5, 10, and 12 m, respectively. As shown in Fig. 7, the smaller the radius, the lower the frequency and the more significant the difference in micro-acceleration produced by the two types of motion. The micro-acceleration generated by the VPMTs is more significant than that generated by linear motion, with a more pronounced difference for smaller radius and lower frequency. At $r = 1$ m and $f = 0.01$ Hz, the acceleration generated by the VPMTs was 9.500×10^{-3} m/s^2, while the acceleration generated by the corresponding linear motion was 3.828×10^{-6} m/s^2, an increase times of 2.481×10^3, equivalent to the acceleration generated by a linear motion with a displacement of 2406.391 mm. Even at $r = 12$ m and $f = 0.1$ Hz, the minimum acceleration enhancement can still reach 0.069 times.

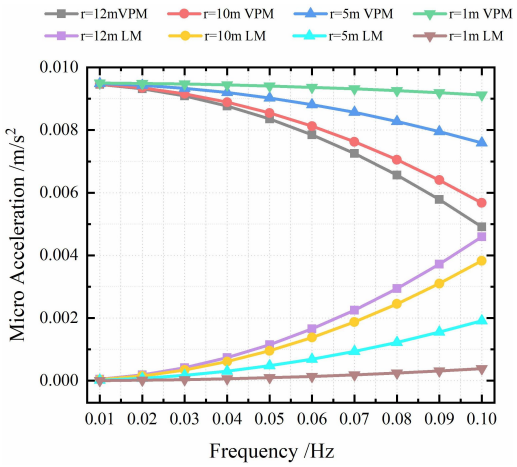

Fig. 7. VPMTs with different radii around the x-axis and corresponding linear acceleration (VPM means virtual pendulum motion; LM means linear motion).

Table 1 displays the increase times in acceleration of the pendulum motion as compared to linear motions for the same displacement.

Table 1. The acceleration of VPMTs compared to LMs for the same pendulum displacement is increased by a factor of magnitude.

f [Hz]	$r = 1$ [m]	$r = 5$ [m]	$r = 10$ [m]	$r = 12$ [m]
0.01	2.481×10^3	4.945×10^2	2.463×10^2	2.049×10^2
0.02	6.187×10^2	1.221×10^2	6.007×10^1	4.972×10^1
0.03	2.739×10^2	5.317×10^1	2.559×10^1	2.099×10^1
0.04	1.532×10^2	2.903×10^1	1.352×10^1	1.093×10^1
0.05	9.731×10^1	1.786×10^1	7.931×10^0	6.276×10^0
0.06	6.697×10^1	1.179×10^1	4.897×10^0	3.747×10^0
0.07	4.867×10^1	8.134×10^0	3.067×10^0	2.222×10^0
0.08	3.679×10^1	5.759×10^0	1.879×10^0	1.233×10^0
0.09	2.865×10^1	4.130×10^0	1.065×10^0	5.543×10^{-1}
0.1	2.283×10^1	2.965×10^0	4.827×10^{-1}	6.896×10^{-2}

4.2. Calibration results

The sensitivity amplitudes S_x and S_y of the sensor along the x- and y-axis directions are the ratio of their output peak-to-peak value V_x, V_y and the peak value of the excitation acceleration a_0 respectively, as defined in ISO 16063-1 [32] and ISO 16063-11 [33]. Based on (1), S_x and S_y are calculated by

$$\begin{bmatrix} S_x \\ S_y \end{bmatrix} = \begin{bmatrix} g_x - \ddot{A} & 0 \\ 0 & g_x - \ddot{A} \end{bmatrix}^{-1} \begin{bmatrix} V_x \\ V_y \end{bmatrix}. \tag{13}$$

In order to verify the reliability of micro-vibration calibration based on the VPMTs of Stewart platform, a quartz flexure accelerometer (6.5 kg) with unknown sensitivity was chosen to perform calibration experiments based on the Stewart platform and rotating platform, respectively. Given the circle radius, the measurement system measures the swing displacement of the VPMTs to calculate the acceleration, and the voltage of the sensor is obtained through the DAQ card to get the sensitivity amplitude. The calibration process of the vibration sensor is shown in Fig. 8.

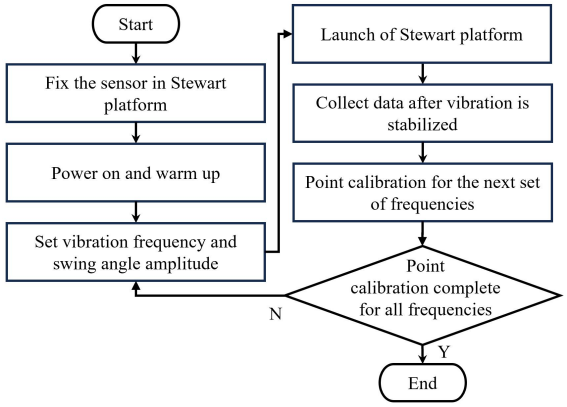

Fig. 8. Diagram of vibration sensor calibration process.

In the range from 0.01 to 0.1 Hz, 10 times calibrations of the sensitivity amplitude were performed at different frequency intervals of 0.01 Hz. The *relative standard deviation* (RSD) of the sensitivity amplitude, $S_{1,\mathrm{RSD}}$ and $S_{2,\mathrm{RSD}}$, were chosen to characterize the uncertainty of the two calibration methods based on the Stewart and rotating platform, respectively. $S_{1,\mathrm{RSD}}$, $S_{2,\mathrm{RSD}}$ are calculated by

$$\begin{cases} S_{1,\mathrm{RSD}} = \dfrac{S_{1,\mathrm{SD}}}{S_{1,\mathrm{AVG}}} \times 100\% \\ S_{2,\mathrm{RSD}} = \dfrac{S_{2,\mathrm{SD}}}{S_{2,\mathrm{AVG}}} \times 100\% \end{cases}, \tag{14}$$

where $S_{1,\mathrm{AVG}}$, $S_{2,\mathrm{AVG}}$ and $S_{1,\mathrm{SD}}$, $S_{2,\mathrm{SD}}$ are the mean and *standard deviation* (SD) of the sensitivity amplitude, respectively. The calibration results of the VPMTs around the x- and y-axis and the rotating platform are shown in Tables 2 and 3, respectively.

10 calibrations for each frequency under the same measurement conditions [34] were performed. The maximum RSD of micro-vibration calibration results based on the Stewart platform is 6.532×10^{-5} with a minimum value of 8.154×10^{-7}. The maximum value based on the rotating platform is 3.808×10^{-5} and the minimum is 5.244×10^{-7}. The above results indicate that the calibration output characteristics of the two platforms have high consistency.

Table 2. Results of a VPMTs sensor calibration around the x-axis (mV/(m/s^2)).

f [Hz]	Stewart platform calibration		Rotating platform calibration		Relative deviation
	Results	$S_{1,RSD}$	Results	$S_{2,RSD}$	
0.01	65.565	2.151×10^{-6}	65.296	4.219×10^{-6}	0.411%
0.02	65.379	4.629×10^{-5}	65.295	2.229×10^{-6}	0.129%
0.03	65.506	5.194×10^{-5}	65.292	5.244×10^{-7}	0.328%
0.04	65.498	2.526×10^{-6}	65.307	2.546×10^{-6}	0.292%
0.05	65.543	3.831×10^{-6}	65.312	1.190×10^{-5}	0.354%
0.06	65.467	2.525×10^{-6}	65.306	6.347×10^{-6}	0.246%
0.07	65.413	3.946×10^{-5}	65.309	1.558×10^{-5}	0.160%
0.08	65.328	1.368×10^{-6}	65.307	3.028×10^{-5}	0.033%
0.09	65.348	1.125×10^{-5}	65.304	3.808×10^{-5}	0.066%
0.1	65.342	1.318×10^{-5}	65.307	2.486×10^{-5}	0.053%

Table 3. Results of a VPMTs sensor calibration around the y-axis (mV/(m/s^2)).

f [Hz]	Stewart platform calibration		Rotating platform calibration		Relative deviation
	Results	$S_{1,RSD}$	Results	$S_{2,RSD}$	
0.01	63.096	8.154×10^{-7}	63.043	4.069×10^{-6}	0.085%
0.02	63.084	5.647×10^{-6}	63.021	2.217×10^{-6}	0.099%
0.03	63.032	6.532×10^{-5}	63.014	3.563×10^{-6}	0.029%
0.04	63.048	4.714×10^{-6}	63.008	3.573×10^{-6}	0.062%
0.05	63.195	7.049×10^{-6}	63.009	4.199×10^{-6}	0.295%
0.06	63.059	1.676×10^{-5}	63.007	2.918×10^{-6}	0.082%
0.07	63.043	1.775×10^{-5}	63.008	6.657×10^{-6}	0.055%
0.08	63.075	2.376×10^{-5}	63.008	1.197×10^{-5}	0.106%
0.09	63.057	6.515×10^{-5}	63.009	9.538×10^{-6}	0.075%
0.1	63.068	5.579×10^{-6}	63.008	3.702×10^{-5}	0.095%

Figures 9a and 10a depict the sensitivity calibration results of the sensors based on the VPMTs of the Stewart platform around the x- and y-axis in the frequency range of 0.01 to 0.1 Hz, respectively, as well as the comparison with the rotating platform calibration results. As can be seen from the figure, the maximum RD of the sensitivity amplitude calibration results of the VPMTs around the x- and y-axis with the rotating platform are 0.411% and 0.295%, respectively, which indicates that the calibration results of the two methods are highly consistent. The validity of the sensitivity calibration of the Stewart platform sensor is verified.

Figures 9b and 10b represent the RSD of the results of the two methods for 10-time sensitivity amplitude calibration in different axial directions, respectively. In both axes, the maximum RSD is of the order of 10^{-5}, which indicates that the dispersion of the results of the two methods relative to their average values is very low and the precision is very high, which verifies the reliability of the sensitivity calibration of the Stewart platform sensor.

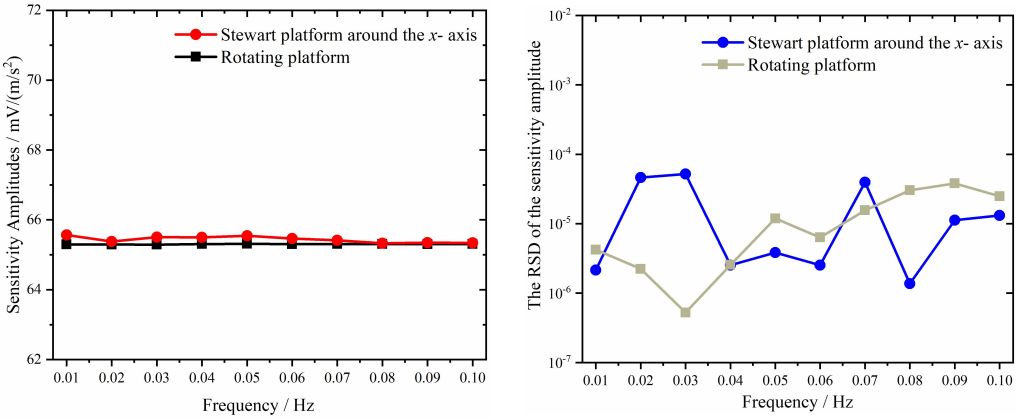

Fig. 9. Calibration results around x-axis compared between Stewart platform and Rotating platform: (a) Sensitivity amplitude; (b) RSD of 10 times calibrations.

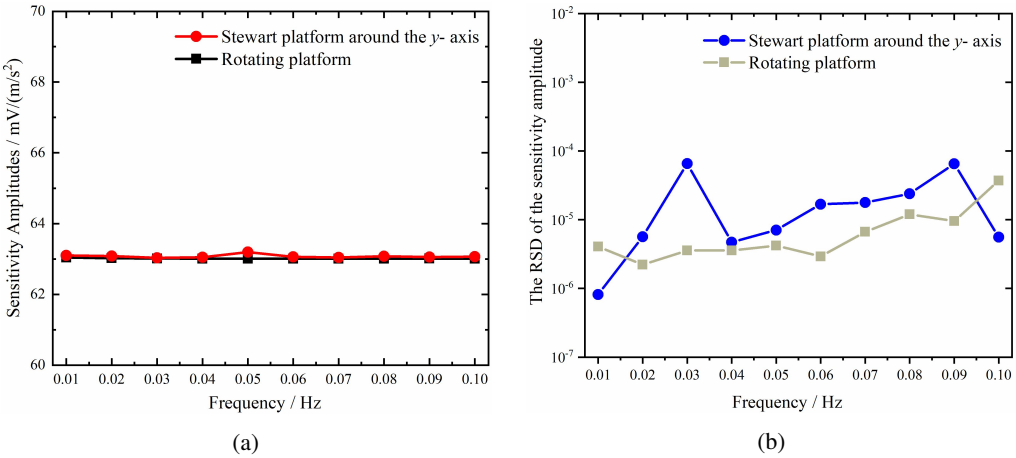

Fig. 10. Calibration results around y-axis compared between Stewart platform and Rotating platform: (a) Sensitivity amplitude; (b) RSD of 10 times calibrations.

5. Conclusions

This study proposed a novel calibration method based on the Stewart platform with the VPMTs which can calibrate the ultra-low frequency conditions at the micro-acceleration from 10^{-5} to 10^{-3} m/s^2 by changing the pendulum motion direction and the pendulum radius within 12 m. Compared with the traditional rotating platform method, the maximum relative deviations of the sensitivity amplitude calibration for pendulum motion around the x- and y-axis are 0.411% and 0.295%, respectively. These results confirmed that Stewart platform-based calibration method has the better reliability and effectiveness for the ultra-low frequency sensor calibration. In addition, it is proved that the pendulum motion can produce the greater micro-acceleration than linear motion for the sensors at the same frequency with the consistent vibration displacement. To achieve the

same micro-acceleration, linear motors need to have a larger stroke, and the maximum stroke needs to reach 2 m, which will undoubtedly increase the cost of manufacturing, and place restrictions on the eventual industrialization of shakers.

Certainly, further work should be addressed in the future, including realizing the VPMTs in any direction in space, optimizing measurement methods to obtain more accurate virtual pendulum parameters, so that the developed method can gradually become a calibration method suitable for most micro vibration sensors, replacing traditional pendulum tables and linear vibration tables.

Acknowledgements

This work was supported by National Natural Science Foundation of China (No. 52075512) and the Fundamental Research Funds for the National Institute of Metrology of China (No. AKYZD2302).

References

[1] Lei, Y., Li, R., Chen, R., Zhang, L., Hu, P., Huang, Q. & Fan, K. (2021). A high-precision two-dimensional micro-accelerometer for low-frequency and micro-vibrations. *Precision Engineering, 67*, 419–427. https://doi.org/10.1016/j.precisioneng.2020.10.011

[2] Shao, S., Song, S., Xu, M., Xie, S., & Li, L. (2016). A piezo-driven micro-inclination stage for calibration of a micro-acceleration transducer: structure and control strategy. *Measurement Science and Technology*, *27*(2). https://doi.org/10.1088/0957-0233/27/2/025008

[3] Jiao, X., Zhang, J., Li, W., Wang, Y., Ma, W. & Zhao, Y. (2023). Advances in spacecraft micro-vibration suppression methods. *Progress in Aerospace Sciences*, *138*. https://doi.org/10.1016/j.paerosci.2023.100898

[4] Ding, J., Wang, Y., Wang, M., Sun, Y., Peng, Y., Luo, J. & Pu, H. (2022). An active geophone with an adjustable electromagnetic negative stiffness for low-frequency vibration measurement. *Mechanical Systems and Signal Processing*, *178*. https://doi.org/10.1016/j.ymssp.2022.109207

[5] He, W., Wang, Z., Mei, Y. & Shen, R. (2013). A novel vibration-level-adjustment strategy for ultralow-frequency vibration calibration based on frequency-shifted method. *Measurement Science and Technology*, *24*(7). https://doi.org/10.1088/0957-0233/24/2/025007

[6] Zhang, H., Duan, B., Wu, L., Hua, Z., Bao, Z., Guo, N., Ye, Y., DeLuca, L. T. & Shen, R. (2021). Development of a steady-state microthrust measurement stand for microspacecrafts. *Measurement*, *178*, 109357. https://doi.org/10.1016/j.measurement.2021.109357

[7] Shimoda, T., Kokuyama, W. & Nozato, H. (2023). Primary microvibration standards down to 10^{-3} m s^{-2} at low frequency. *Measurement Science and Technology*, *34*(9). https://doi.org/10.1088/1361-6501/acd570

[8] Scott, D. A. & Dickinson, L. P. (2014). Distortion effects in primary calibration of low-frequency accelerometers. *Metrologia*, *51*(3), 212–224. https://doi.org/10.1088/0026-1394/51/3/212

[9] Yang, M., Wang, Y., Cai, C., Liu, Z., Zhu, H. & Zhou, S. (2019). Monocular vision-based low-frequency vibration calibration method with correction of the guideway bending in a long-stroke shaker. *Opt Express*, *27*(11), 15968–15981. https://doi.org/10.1364/OE.27.015968

[10] Yang, M., Wang, Y., Liu, Z., Zuo, S., Cai, C., Yang, J. & Yang, J. (2022). A monocular vision-based decoupling measurement method for plane motion orbits. *Measurement*, *187*. https://doi.org/10.1016/j.measurement.2021.110312

[11] Yang, M., Liu, W., Liu, Z., Cai, C., Wang, Y. & Yang, J. (2023). Binocular Vision-Based Method Used for Determining the Static and Dynamic Parameters of the Long-Stroke Shakers in Low-Frequency Vibration Calibration. *IEEE Transactions on Industrial Electronics*, *70*(8), 8537–8545. https://doi.org/10.1109/tie.2022.3208559

[12] Yicai He, J. L., Junzhe Zhao. (2017). Calibrate of Ultra-low Frequency Acceleration by Mathematical Pendulum-vibration Generator Method. *Acta Metrologica Sinica*, *38*(4), 424–428. https://doi.org/10.3969/j.issn.1000-1158.2017.04.09 (in Chinese)

[13] Lei Xiong, H. O., Jianping Liao, Yicai He. (2015). The Dynamic Calibration of Linear Accelerometer at Different Range. *Journal of Projectiles, Rockets, Missiles and Guidance*, *35*(4), 149–153. (in Chinese)

[14] Poorghasem, S. & Bao, Y. (2023). Review of robot-based automated measurement of vibration for civil engineering structures. *Measurement*, *207*, 112382. https://doi.org/10.1016/j.measurement.2022.112382

[15] Gaitan, M., & Geist, J. (2022). Calibration of triaxial accelerometers by constant rotation rate in the gravitational field. *Measurement*, *189*, 110528. https://doi.org/10.1016/j.measurement.2021.110528

[16] Yang, M., Liu, Z., Cai, C., Wang, Y., Yang, J. & Yang, J. (2022). Monocular Vision-Based Calibration Method for the Axial and Transverse Sensitivities of Low-Frequency Triaxial Vibration Sensors with the Elliptical Orbit Excitation. *IEEE Transactions on Industrial Electronics*, *69*(12), 13763-13772. https://doi.org/10.1109/tie.2021.3130325

[17] Liu, Z., Cai, C., Yu, M. & Dong, M. (2018). Testing of Accelerometer Transverse Sensitivity Using Elliptical Orbits. *Mapan*, *33*(3), 217–226. https://doi.org/10.1007/s12647-018-0255-7

[18] Deka, S., Pallekonda, R. B. & Rahang, M. (2021). Comparative assessment of modified deconvolution and neuro-fuzzy technique for force prediction using an accelerometer balance system. *Measurement*, *171*, 108770. https://doi.org/10.1016/j.measurement.2020.108770

[19] Yang, Q., Cai, C., Yang, M., Kong, M., Liu, Z. & Liang, F. (2023). Dynamic tilt testing of MEMS inclinometers based on conical motions. *Metrology and Measurement Systems*, *30*(1), 31–47. https://doi.org/10.24425/mms.2023.144398

[20] Yu, M., Liu, A.-D., Ma, M.-D., Yang, L.-F. & Hu, H.-B. (2011). Magnitude and phase measurement technology for ultra-low frequency vibration using laser interferometry. *Zhendong yu Chongji/Journal of Vibration and Shock*, *30*(11), 130–134. (in Chinese)

[21] Palmieri, P. (2009). A Phenomenology of Galileo's Experiments with Pendulums. *The British Journal for the History of Science*, *42*(4), 479–513. http://www.jstor.org/stable/25592307

[22] Koleda, P., Hrčková, M. & Adamik, M. (2016). Identification of pendulum oscillation parameters using mems accelerometer. *MM Science Journal*, *2016*, 1134–1140.

[23] Hao, H., Wei, Z., He, H. & Liu, L. (2021). Development of laser-based system to determine fault surface morphology at the micron scale. *Measurement*, *180*, 109498. https://doi.org/10.1016/j.measurement.2021.109498

[24] Zhihua Liu, C. C., Mei Yu, Yan Xia, Jingsheng Li. (2017). Relative motion in comparative calibration of piezoelectric accelerometers. *Metrology Technology*, *5*(12). https://doi.org/10.3969/j.issn.1000-0771.2017.12.0 (in Chinese)

[25] Kokuyama, W., Shimoda, T. & Nozato, H. (2022). Primary accelerometer calibration with two-axis automatic positioning stage. *Measurement*, *204*, 112044. https://doi.org/10.1016/j.measurement.2022.112044

[26] Zhao, K., Liu, Z., Cai, C., Bao, F., Tu, C. & Qi, Y. (2023). Design and calibration of the 6-DOF motion tracking system integrated on the Stewart parallel manipulator. *Optics Express*, *32*(1). https://doi.org/10.1364/oe.510804

[27] Fu, L., Liu, Z., Cai, C., Tao, M., Yang, M. & Huang, H. (2023). Joint space-based optimal measurement configuration determination method for Stewart platform kinematics calibration. *Measurement*, *211*. https://doi.org/10.1016/j.measurement.2023.112646

[28] Fu, L., Yang, M., Liu, Z., Tao, M., Cai, C. & Huang, H. (2022). Stereo vision-based Kinematic calibration method for the Stewart platforms. *Opt Express*, *30*(26), 47059–47069. https://doi.org/10.1364/OE.479597

[29] Liu, Z., Cai, C., Yu, M. & Yang, M. (2017). Applying Spatial Orbit Motion to Accelerometer Sensitivity Measurement. *IEEE Sensors Journal*, *17*(14), 4483–4491. https://doi.org/10.1109/jsen.2017.2703859

[30] Huang, T., Zhao, D., Yin, F., Tian, W. & Chetwynd, D. G. (2019). Kinematic calibration of a 6-DOF hybrid robot by considering multicollinearity in the identification Jacobian. *Mechanism and Machine Theory*, *131*, 371–384. https://doi.org/10.1016/j.mechmachtheory.2018.10.008

[31] Yang, L., Tian, X., Li, Z., Chai, F. & Dong, D. (2019). Numerical simulation of calibration algorithm based on inverse kinematics of the parallel mechanism. *Optik*, *182*, 555–564. https://doi.org/10.1016/j.ijleo.2019.01.079

[32] International Organization for Standardization. (1998). *Methods for the calibration of vibration and shock transducers – Part 1: Basic concepts* (ISO Standard No. 16063–1). https://www.iso.org/standard/25043.html

[33] International Organization for Standardization. (1999). *Methods for the calibration of vibration and shock sensors – Part 11: Primary vibration calibration by laser interferometry* (ISO Standard No. 16063–11). https://www.iso.org/standard/24951.html

[34] Liu, W., Yang, M., Cai, C., Liu, Z. & Yang, J. (2023). Dynamic calibration method of digital angular vibration sensor based on machine vision. *Journal of Vibration and Shock*, *42*(13), 177–182. http://jvs.sjtu.edu.cn/EN/Y2023/V42/I13/177 (in Chinese)

Tong Ye received the B.E. degree from the College of Information Engineering, Lingnan Normal University, Zhanjiang, China, in 2021. At present, she is studying for a Master's degree at the College of Metrology and Measurement Engineering, China Jiliang University, Hangzhou, China. Her main research interests include robotics and micro-vibration calibration.

Chenguang Cai received his Ph.D. degree in Precision Instrumentation and Mechanics from the School of Instruments Science and Optoelectronic Engineering, Beihang University, Beijing, China, in 2007. From 2007 to 2009, he worked for the Nokia Research Center (Beijing) as a Post doctor. He is currently a research fellow at the National Institute of Metrology, Beijing, China. He was a visiting scientist in Physikalisch-Technische Bundesanstalt (PTB), Germany, in 2016. He is interested in vibration calibration and optics measurement.

Zhihua Liu received the B.E. degree in Mechanical Engineering from Jilin University, Changchun, China, in 2010, and the Ph.D. degree in Mechanical Engineering from Tsinghua University, Beijing, China, in 2015. He was a visiting scientist at the Physikalisch-Technische Bundesanstalt (PTB) in Braunschweig, Germany, in 2018. He is currently a vice research fellow at National Institute of Metrology, China. His research interests include mechanisms and robotics.

Fubing Bao received the B.Sc. and Ph.D. degrees in Mechanics Engineering from Zhejiang University, in 2003 and 2008, respectively. He is currently a Full Professor at the Department of Measurement and Control Technology and Instrumentation of China Jiliang University. He has coauthored 1 book and 100 journal publications. His current research interests include vibration calibration of the sensors and measurement.

Fei Xu received his Ph.D. degree in Engineering Thermophysics from the Harbin Institute of Technology. Currently, he is a lecturer at the College of Metrology and Measurement Engineering, China Jiliang University, Hangzhou, China. His research interests include heat and mass transfer measurement and control and industrial big data.

Xiangkun Lian received his master's degree from the College of Metrology and Measurement Engineering, China Jiliang University, Hangzhou, China., majoring in electronic information. His main research interest is reciprocal method calibration..